Available online at www.sciencedirect.com
ScienceDirect
Polymer 48 (2007) 1316–1328
polymer
www.elsevier.com/locate/polymer

Domain nucleation dictates overall nanostructure in composites of block copolymers and model nanorods

Castro S.T. Laicer, Randy A. Mrozek, T. Andrew Taton*

Department of Chemistry, University of Minnesota, 207 Pleasant Street SE, Minneapolis, MN 55455, United States

Received 30 October 2006; received in revised form 22 December 2006; accepted 31 December 2006
Available online 8 January 2007

Abstract

The detailed nanostructure of composites formed from block copolymers and nanoparticles is known to depend sensitively on the preferred morphology of the block copolymer, on the shapes of the particles, and on interactions between the two components. But it can also depend on the kinetics of self-assembly in the polymer, and there are circumstances under which the kinetics of morphologically selective domain nucleation and growth determine the overall nanostructure of the composite. To study the mechanism of morphological seeding in block-copolymer nanocomposites, we have combined cylinder phases of polystyrene-*block*-polyisoprene diblock (as a solution in dibutylphthalate) and poly(styrene-*block*-isoprene-*block*-styrene) triblock (as a blend with homopolystyrene) copolymers with gold nanorods of different diameters and surface treatments. Polarized optical microscopy and transmission electron microscopy on these composites demonstrate that the nanorods selectively nucleate coaxial domains of copolymer cylinders (i.e., domains of cylinders aligned along the same axis as the nanorod). These single nucleation events occur regardless of nanorod diameter and surface character, and determine the order of most of the surrounding polymer. Mesoscale modeling of the nucleation process, performed with nanorods of different diameters and with different polymer–surface interactions, illustrates the mechanism by which copolymer-dispersed nanorods with different sizes and surface chemistry can template the organization of cylindrical copolymer domains.

Keywords: Block copolymers; Nanorods; Nucleation

1. Introduction

When block copolymers are cooled below a characteristic order-to-disorder transition temperature (T_{ODT}), they spontaneously assemble into nanostructured phases in which the polymer blocks are segregated into periodic motifs [1–3]. Even the simplest diblock copolymers form a rich variety of segregated morphologies, including lamellar, hexagonal (cylindrical), gyroid, and cubic (spherical) structures. In bulk material, order develops by a process of nucleation and growth of individual, incoherently organized domains, such that the material is locally ordered (on the micron scale) but globally disordered [4–10]. Recent research has explored the possibility of generating coherent domain orientation, and thus extended the order, by interactions with a nanostructured surface. When block-copolymer materials in contact with a nanostructured surface are cooled or annealed below T_{ODT}, organization of the morphology can be epitaxially related to the surface nanostructure. For example, it has been shown that the individual lamellae of lamellar-phase block-copolymer orient with lithographically patterned stripes when pattern periodicities are commensurate with the copolymer *d*-spacing [11–13]. Likewise, etched nanoscopic grooves or edges template the organization of spheres, cylinders or lamellae in block-copolymer films [14–17]. The impact of surface nanostructure on the overlying copolymer morphology can be thermodynamic, achieved by annealing the material near T_{ODT} over long periods of time. But surface templating can also be kinetic, where organization due to initial, selective wetting of one copolymer block onto the surface pattern propagates into the bulk material. The depth of epitaxial ordering away from

* Corresponding author. Tel.: +1 612 626 4681; fax: +1 612 626 7541.
E-mail address: taton@chem.umn.edu (T.A. Taton).

0032-3861/$ - see front matter © 2007 Elsevier Ltd. All rights reserved.
doi:10.1016/j.polymer.2006.12.056

a flat surface is typically shallow (100 nm–10 μm); as a result, three-dimensional monoliths of block copolymer cannot be uniformly ordered by lithographic patterns.

In principle, similar epitaxial ordering could be kinetically induced at the surfaces of colloidal nanostructures dispersed throughout a bulk block-copolymer sample. For example, Thomas et al. have shown that clay particles template domains in roll-cast oriented films of poly(styrene-*block*-isoprene-*block*-styrene) [18] and poly(styrene-*block*-butadiene-*block*-styrene) triblock copolymers [19]. Kinetic studies by Krishnamoorti et al. on block-copolymer blends of poly(styrene-*block*-ethylene-*co*-butene-1-*block*-styrene) and poly(styrene-*block*-ethylene-*co*-butene-1) showed dramatic enhancements in ordering kinetics of spherical domains [20,21]. In these studies, large silicate particles (thickness = 0.95 nm, $d \sim 0.50$–10 μm) acted as kinetic seeds for spherical domains [20,21], while small silicate particles ($d \sim 30$ nm) did not influence the ordering kinetics of the block-copolymer blend [21]. By contrast, the same silicate particles did not influence the ordering kinetics of cylindrical domains, leading the authors to conclude that for particles to serve as effective templates, they should promote the symmetry of copolymer domains and be considerably larger than the nascent domain nucleus [20,21]. By contrast, Hasegawa and Usuki showed that relatively small clay particles (thickness ~ 1 nm, $l \sim 200$ nm) templated domains in poly(styrene-*block*-ethylene-*co*-butene-1-*block*-styrene) [22]. Although the authors did not determine the morphology of their block copolymer, the nucleated domains presumably consisted of polystyrene (PS) cylinders since the composition of PS segments was 30 wt% [22]. Additionally, Lee et al. showed that the alignment of cylindrical domains by large amplitude oscillatory shear was diminished with addition of clay particles [23].

Recently, we extended this concept to demonstrate that suspended nanorods ($d = 180$ nm, $l = 3$–6 μm) nucleate the growth of micron-scale, cylindrical-phase domains in solutions of poly(styrene-*block*-isoprene) (SI) in dibutylphthalate (DBP) that were cooled below T_{ODT} [24]. Furthermore, we showed that the orientation of these nucleated domains was dictated by the long axis of the Au nanorod nucleants [24]. The mechanism of epitaxial ordering in these materials, however, was not clear from our initial studies. Here, we propose a mechanism for co-alignment of cylindrical domains in which initial wetting of the nanorod surface by a copolymer lamella is followed by templated growth of a domain from this layer (Scheme 1). One feature of this proposed mechanism is that domain seeding should occur for any nanorod–copolymer mixture in which the nanorod surface is selectively wet by the copolymer, and in which surface curvature is sufficient to direct the conversion of the wetting layer to segregated copolymer cylinders. To test this hypothesis, we investigated the effects of nanorod diameter and polymer–surface interactions on domain nucleation in SI–DBP solutions using polarized optical microscopy. Consistent with the mechanism in Scheme 1, we found that selective interactions between either the styrene or isoprene block and the nanorod surface are sufficient to template the organization of the surrounding

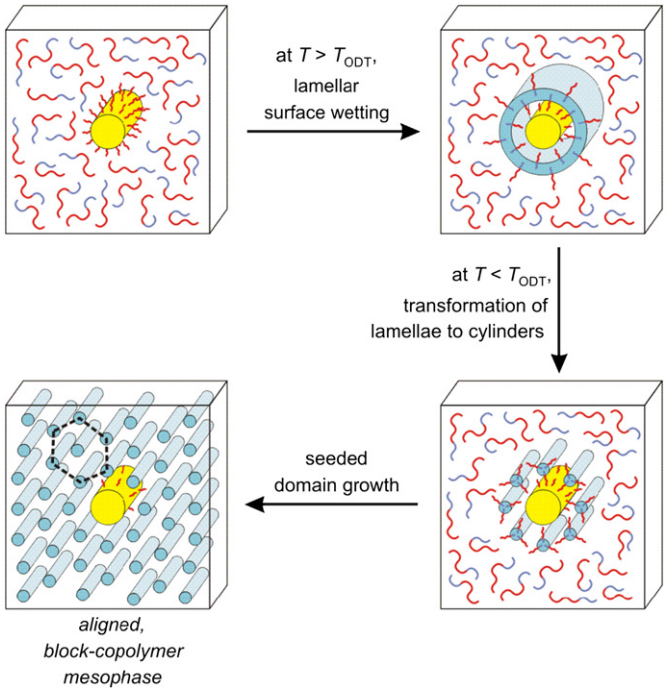

Scheme 1.

cylindrical mesophase, and that a wide range of nanorod diameters can successfully seed cylinder-phase domains. Because it was extremely difficult to cryotome and image SI–DBP by transmission electron microscopy (TEM) due to its fluidity, we verified nanorod-directed domain organization by TEM in a related blend of SIS triblock copolymer, polystyrene (PS) homopolymer, and Au nanorods. Mesoscale modeling of block-copolymer domain growth in the presence of templating nanorods with different diameters and surface properties supports the stepwise mechanism, and illustrates that nucleation kinetics can determine the morphology of block-copolymer nanocomposites.

2. Experimental

2.1. Materials

Both SI diblock and SIS triblock copolymers were investigated in this study. SI ($M_n = 2.98 \times 10^4$ g/mol; $M_w/M_n = 1.02$), with polystyrene and polyisoprene block molecular weights (M_n) of 18 and 12 kg/mol, respectively, was purchased from Polymer Source, Inc. (Dorval, Canada). SI polymer solutions in DBP (Aldrich) were prepared following a previously published procedure [24]. SIS ($M_n = 1.28 \times 10^5$ g/mol; $M_w/M_n = 1.11$), containing 18 wt% styrene, was donated by Dexco Polymers (Vector 4111). Samples were prepared by dissolving SIS (1 wt%) and antioxidant (2,6-di-*tert*-butyl-4-methylphenol, Aldrich) (0.1 wt%) in CH_2Cl_2. The solution was filtered through a PTFE filter (0.20 μm) and stirred under a nitrogen purge for two days. The concentrated polymer was annealed in a vacuum oven for four days at 60 °C. SIS–PS blends were prepared by dissolving pre-weighed amounts of

filtered SIS and polystyrene ($M_w = 1300$ g/mol; $M_w/M_n = 1.06$, Alfa Aesar) in CH_2Cl_2. Samples were then stirred under a nitrogen purge for two days and annealed in a vacuum oven for two days at 60 °C to give SIS–PS blends with a composition of 86 wt% SIS and 14 wt% PS.

2.2. Gold nanorod synthesis

Gold nanowires were prepared by electroless reduction of $Na_3Au(SO_3)_2$ gold plating solution (Oromerse SO Part B, Technic Inc.) in track-etched polycarbonate membranes (Whatman) with 15, 50, 80, and 400 nm pore diameters and 6 μm pore length, following a previously published procedure [24]. Diameters of the resulting nanorods, as determined by scanning electron microscopy (SEM), were 30, 100, 180, and 400 nm, respectively. Consistent with previously published syntheses [25], the measured diameters of the Au nanowires were larger than the reported nominal pore sizes of the membrane hosts. Au suspensions are hereafter denoted by "Au_d", where d is the measured diameter of the Au nanowires. Nanowires were isolated by dissolving the membrane hosts in 10–20 mL CH_2Cl_2.

2.3. Surface modification of gold nanowires

Nanowires were functionalized with organothiols following a modified version of a previously published procedure [24]. For example, 1-dodecanethiol (40 μL) was added to Au nanowire suspensions and solutions were mixed on a mechanical shaker for 20 h at room temperature. In the case of $C_{12}H_{25}S$–Au_{100}, $C_{12}H_{25}S$–Au_{180}, and $C_{12}H_{25}S$–Au_{400}, nanowire suspensions were allowed to settle by gravity, washed repeatedly, and resuspended in fresh CH_2Cl_2. Final suspension volumes were 15 mL for $C_{12}H_{25}S$–Au_{100} and 10 mL for $C_{12}H_{25}S$–Au_{400}. Suspensions of $C_{12}H_{25}S$–Au_{30} nanowires were centrifuged at 735× g for 7 min and the clear supernatant was decanted. Fresh CH_2Cl_2 (15 mL) was added and Au_{30} nanowires were resuspended by brief sonication (2 s). The concentrations of the resulting Au nanowire suspensions were determined at this stage by oxidative etching of an aliquot of the rod suspension, followed by quantitation of the product Au ions in solution by ICP-MS. Calculated concentrations were 4.37×10^8 Au rods/mL (1.81×10^{-4} M Au^{3+} by ICP-MS) for $C_{12}H_{25}S$–Au_{30}, 1.14×10^8 Au rods/mL (5.26×10^{-4} M Au^{3+}) for $C_{12}H_{25}S$–Au_{100}, and 2.86×10^6 Au rods/mL (2.11×10^{-4} M Au^{3+}) for $C_{12}H_{25}S$–Au_{400}. Extinction coefficients measured from UV–vis spectroscopy were $\varepsilon_{518}(Au_{30}) = 6.44 \times 10^{11}\ M^{-1}\,cm^{-1}$ and $\varepsilon_{623}(Au_{100}) = 3.83 \times 10^{12}\ M^{-1}\,cm^{-1}$ (where M^{-1} = L/mol Au rods). $\varepsilon_{580}(Au_{180}) = 5.84 \times 10^{12}\ M^{-1}\,cm^{-1}$ was determined previously [24]. These extinction coefficients were used to confirm nanorod concentrations in experiments with these three nanorods [26]. Benzyl-modified Au nanorods were prepared by substituting benzyl mercaptan (10 μL) for the dodecanethiol used in the procedure described above for $C_{12}H_{25}S$–Au. Concentrations of $PhCH_2S$–Au_{180} (5.26×10^7 Au rods/mL, 7.87×10^{-4} M Au^{3+}), and of bare Au_{180} (3.12×10^7 Au rods/mL, 4.66×10^{-4} M Au^{3+}), were determined by UV–vis spectroscopy and calculated using $\varepsilon_{580}(Au_{180})$ [24].

2.4. SI–DBP composite materials

Composite samples were prepared by titrating CH_2Cl_2 suspensions of Au nanowires into pre-weighed amounts of SI–DBP. Samples were then stirred under a nitrogen purge until a gravimetric endpoint was reached. Final Au nanowire concentrations in SI–DBP were calculated to be 3.40×10^8 rods/g SI–DBP for $C_{12}H_{25}S$–Au_{30}, 3.06×10^7 rods/g for $C_{12}H_{25}S$–Au_{100}, and 2.86×10^6 Au rods/g for $C_{12}H_{25}S$–Au_{400}. Samples of SI–DBP with bare Au_{180} and $PhCH_2S$–Au_{180} nanorods were prepared similarly to yield concentrations of 2.22×10^6 Au rods/g SI–DBP for both [27]. Samples of SI–DBP with carbon nanofibers (Pyrograf Products, Inc., Cedarville, OH; Pyrograf III® Carbon Fiber, LHT Grade; average d: 200 nm) were prepared similarly [27].

2.5. SIS–PS–Au composite materials

Composite materials from SIS–PS blends were prepared by titrating a CH_2Cl_2 suspension of 1-dodecanethiol-modified Au_{180} nanowires (2.98×10^8 Au rods/mL, 7.05×10^{-4} M) into a pre-weighed amount of an SIS–PS blend. The sample was dried by stirring under a nitrogen purge and annealed in a vacuum oven for 19 h at 45 °C.

2.6. Scanning electron microscopy (SEM)

SEM images were obtained with a Hitachi S-800 field-emission gun scanning electron microscope at an accelerating voltage of 5.0 kV.

2.7. Polarized optical microscopy (POM)

POM analysis of domain growth in SI–DBP–Au samples was performed with a Nikon Optiphot polarized-light microscope fitted with a Brace–Köhler type (1/20 λ) compensator, and a Linkam Scientific Instruments heat stage as described in a previously published procedure [24]. SI–DBP–Au composite samples were first annealed at 55 °C ($T > T_{ODT}$) for at least 5 min prior to a rapid temperature quench to $T < T_{ODT}$. Time-resolved images were collected after samples were quenched and held at constant temperature. Transition temperatures for SI–DBP samples composited with Au_{30} ($T_{ODT} = 46.3$ °C), Au_{100} ($T_{ODT} = 45.8$ °C), and Au_{400} ($T_{ODT} = 46.2$ °C) were determined by the initial disappearance of birefringence in samples that had been first annealed at 40 °C ($T < T_{ODT}$) for 5 min prior to heating at a rate of 0.30 °C/min. POM analysis on SIS–PS–Au samples was performed with an Olympus BX51 polarizing microscope equipped with a 1/10 λ Brace–Köhler compensator. Samples were placed in an Instec HCS402 heat stage and the temperature was controlled by an Instec STC200 heat controller. Samples were sealed between two glass slides with a high-temperature silicone glue. Sample thickness was controlled with 125 μm

PTFE gaskets. Measurements were made on samples that were initially annealed at 215 °C for 2 h and cooled to 25 °C at 0.10 °C/min.

2.8. Small-angle X-ray scattering (SAXS)

SAXS measurements on pure SIS–PS and SIS–PS–Au composite samples were obtained on a 2-D 2m SAXS instrument. Instrumental details for SAXS measurements have been previously published [24]. Measurements were made on samples that had been sealed between Mylar films with a high-temperature silicone glue. Samples were initially measured at room temperature and then heated to 120 °C. Samples were subsequently annealed at this temperature for 30 min prior to measurement. The exposure time for each measurement was 10 min.

2.9. Transmission electron microscopy (TEM)

In a heat stage, composites of SIS–PS and $C_{12}H_{25}S$–Au_{180} nanorods were first annealed at 220 °C ($T \approx T_{ODT}$) for 1 min and then cooled to 120 °C at a rate of 0.10 °C/min. After cooling, the temperature was maintained at 120 °C for at least 5.5 h prior to freezing samples in an ice-water bath. TEM specimens (~65 nm thick) were sliced with a Reichert cryo-ultramicrotome system (Model FC S). The temperature of the glass knife and sample was maintained at approximately −140 °C by continuously purging liquid nitrogen through the sample chamber. TEM specimens were collected on TEM grids and stained with vapors from a 4 wt% osmium tetroxide aqueous solution (OsO_4, Aldrich) for 12 h. TEM images were obtained with a JEOL 1210 transmission electron microscope at an accelerating voltage of 120 kV. In these experiments, composites with high concentrations of nanorods (2.74×10^{-3} Au rods/μm^3 SIS–PS) were used to increase the chance that cryotomed slices would contain a nanorod.

2.10. Mesoscale modeling

Simulations were performed using the MESODYN module of Materials Studio (Accelrys, San Diego, CA). Parameters for the simulations are given in the Supplementary Data.

3. Results and discussion

3.1. Domain seeding in SI–DBP by Au nanorods

Previously, we examined the impact of alkane-functionalized, 180-nm diameter Au nanorods ($C_{12}H_{25}S$–Au_{180}) on domain nucleation in cylinder-phase SI–DBP solutions, and found that the copolymer cylinders in the nucleated domains were coaxially aligned with the seeding nanorods [24]. In that study, we hypothesized that engineering positive surface interactions between one of the copolymer blocks and the nanorod surface, and that matching the diameter of the nanorods to the diameters of the copolymer cylinders, could be important for seeding domain alignment. In this study we investigated the effects of Au nanorod size and surface character on the same SI–DBP solutions. First, three new dodecanethiol-modified Au nanorod suspensions with rod diameters of 30, 100, and 400 nm (Fig. 1) were composited with SI–DBP mixtures with a 22-nm cylinder *d*-spacing. Therefore, Au nanorod sizes ranged from similar to substantially larger than the cylinder periodicity of the copolymer. As in our previous study, the nanorods were functionalized with dodecanethiol to promote selective interactions of PI segments with the nanorod surface. The smallest nanorods we were able to produce by electroless deposition from commercially available polycarbonate membranes were 30 nm in diameter, so we were unable to investigate the seeding effects in nanorods smaller than this. Nevertheless, we found that Au_{30} rods were gradually damaged by breaking during extensive compositing with polymer (Figs. S11 and S12) [27], and we suggest that 30 nm may be a practical lower limit for the diameter of gold nanorods composited by the method described here.

Domain seeding and growth in SI–DBP–Au composites was initiated by cooling samples below T_{ODT} and monitoring the evolution of order by time-lapsed POM. In the absence of nanorods, cooling SI–DBP below T_{ODT} results in a combination of spherulitic (~60%) and "single-crystalline" [28] ellipsoidal (~40%) domains [24]. POM measurements in SI–DBP samples composited with Au_{30}, Au_{100}, and Au_{400} nanorods, on the other hand, showed preferential nucleation of uniformly aligned, ellipsoidal domains when cooled below T_{ODT} under the same conditions (Fig. 2). By annealing samples at constant temperature $T < T_{ODT}$, we observed growth of domains that were up to 200 μm in size (Fig. 2d). As

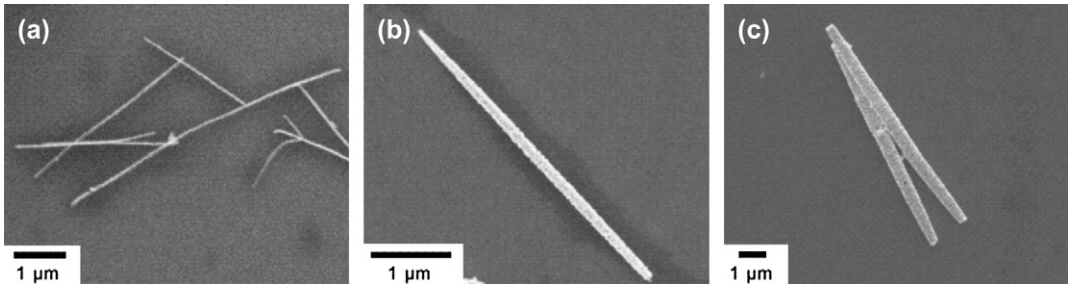

Fig. 1. SEM images of gold nanowires (2–6 μm length) with diameters of (a) 30 nm (b) 100 nm and (c) 400 nm, drop-coated on a silicon wafer substrate and allowed to dry.

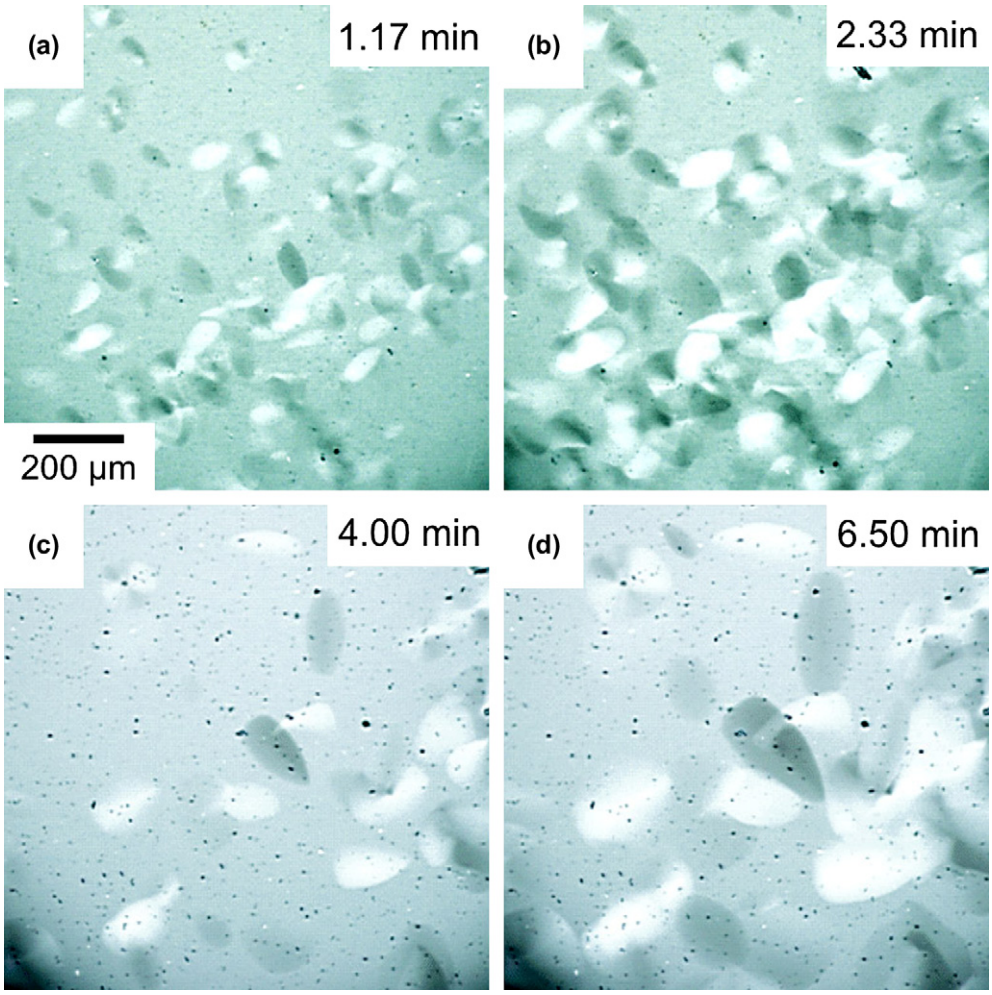

Fig. 2. Time-lapsed POM images of domains nucleated in SI–DBP mixtures composited with 30 nm (a,b) and 400 nm (c,d) diameter Au nanorods. Samples were quenched from $T > T_{ODT}$ to (a,b,c,d) 44.7 °C. Samples were annealed at 55.0 °C for 5 min prior to quenching below T_{ODT}. The number of nanorod nucleants embedded in the volume of polymer shown above is estimated to be 4×10^4 (a,b) and 3×10^2 (c,d)—in both cases, larger than the number of observed domains. The alignment of block-copolymer cylinders within nucleated domains, as well as the corresponding dark and bright shading patterns, are consistent with a previously published report [25]. When samples were annealed at constant temperature after temperature quenches below isotropic phases ($T < T_{ODT}$), we found that secondary domain nucleation events were negligible after initial seeding and growth of domains.

previously shown, heterogeneous nucleation in these samples was indicated by the reappearance of the same domains at identical locations when samples were repeatedly melted and cooled [24]. Most importantly, the preference for nucleating ellipsoid domains in SI–DBP did not vary with Au nanorod size (Fig. 3). When domain types were counted in multiple samples, the overall percentage of ellipsoid domains did not significantly vary with temperature for quenches below $T < 44.5$ °C for all nanorod sizes (Fig. 3b). The *density* of nucleated domains did vary with rod diameter; for example, the number of smaller $C_{12}H_{25}S–Au_{30}$ rods that could be stably composited with SI–DBP was much higher than the number of larger $C_{12}H_{25}S–Au_{400}$ rods, and so the number of nucleated domains in SI–DBP–($C_{12}H_{25}S–Au_{30}$) was consistently greater than in SI–DBP–($C_{12}H_{25}S–Au_{400}$) that had been cooled to the same temperature (Figs. 2 and 3a).

We were surprised to find that all of the gold nanorod diameters we prepared successfully templated homogeneous domains in SI–DBP, and considered the possibility that the results were an artifact of the procedure for preparing the materials. To ensure that domain seeding was not due to some residual material from the nanorod synthesis, as a negative control, we prepared irregular Au nanoparticles from the same polycarbonate membrane templates by prematurely terminating the electroless deposition. SEM images of these particles after isolation from the membrane showed that they were predominantly polydisperse ($d = 20–150$ nm) spherical particles [27]. SI–DBP–Au composites made from these particles exhibited primarily spherulitic domain growth [27]. Overall, these results indicate that the prevalence for seeding homogeneously aligned domains is not affected by the size of Au nanorod nucleants, but that the shape of the nanorod is critical.

We also found that nanorod nucleation was not significantly influenced by surface functionalization of the rods. As mentioned above, we originally functionalized the nanorods with dodecanethiol ligands to induce wetting of the nanorod surface by the polyisoprene block. We had assumed that this would be

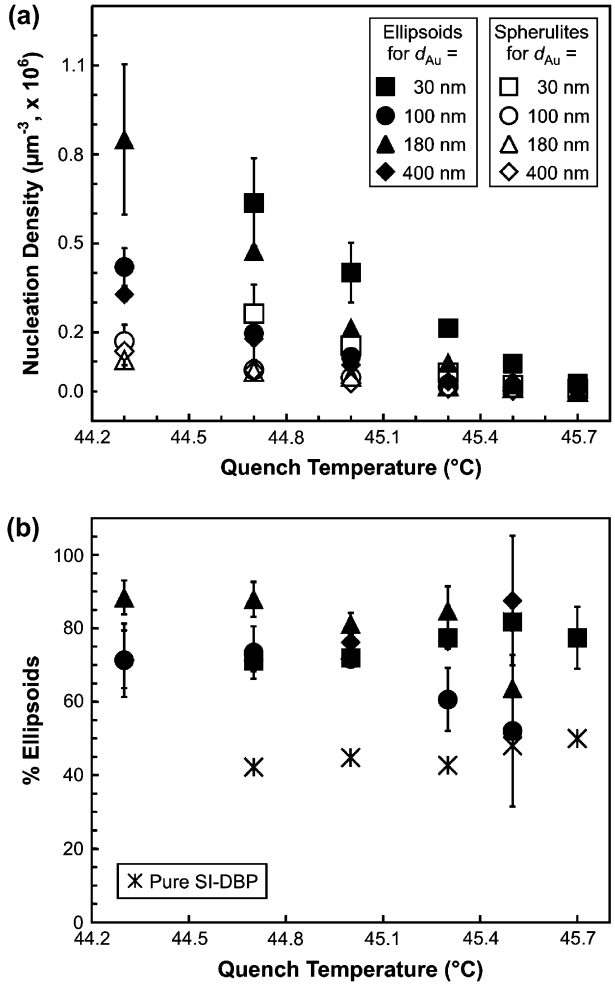

Fig. 3. (a) Nucleation density of ellipsoid and spherulite grains at varying quenching temperatures for SI–DBP composited with $C_{12}H_{25}S$–Au nanorods with diameters of 30, 100, 180, and 400 nm. Previously reported data for SI–DBP–($C_{12}H_{25}S$–Au_{180}) samples are included for comparison [25]. Samples were annealed in the disordered state at 55 °C prior to quenching to each final temperature, and then domains were identified and counted from polarized microscope images. Ellipsoids were identified as domains with uniform, light or dark shading patterns. Spherulites were identified as round-shaped domains with Maltese cross (alternating light and dark) shading patterns. The criteria for identifying spherulites and ellipsoids were based on those previously reported by Chastek and Lodge for SI–DBP [4]. (b) Variation in the fraction of ellipsoidal domains with quenching temperature, calculated from data in (a). Low domain counts are responsible for larger errors at higher quenching temperatures.

important, based on the past studies that showed block-copolymer nanodomains align parallel to flat surfaces with positive surface energies for either copolymer blocks [29–33], but perpendicular to surfaces with no energetic preference for either blocks [34–37]. In this study, however, we found that various Au nanorod surface treatments—including functionalization with polystyrene-wetting aromatic ligands, or even without functionalization—similarly resulted in ellipsoidal, homogeneous domains. POM analysis of SI–DBP–($PhCH_2S$–Au_{180}) and SI–DBP–(Au_{180}) showed the fraction of ellipsoidal domains to be 78% ($T = 44.0$ °C) and 75% ($T = 44.5$ °C), respectively (Fig. S5) [27]. Pyrograf carbon nanorods ($d \approx 200$ nm) also promoted the nucleation of ellipsoid domains when added to the same SI–DBP material, albeit not as strongly (62% ellipsoids, $T = 45.0$ °C). Taken together, these results indicate that nucleation of cylinder domains by nanorods may not be as sensitive to the surface properties of the nucleants as we first predicted.

In all of the experiments described above, the concentration of nanorods was much higher than the density of observed domains. In order to more closely evaluate the nucleation efficiency of the nanorods, we composited SI–DBP with different amounts of $C_{12}H_{25}S$–Au_{180} and cooled the materials through T_{ODT}. Domain nucleation switched from simultaneous nucleation of spherulites and ellipsoids to predominantly ellipsoids over a fairly narrow concentration range, when the concentration of $C_{12}H_{25}S$–Au_{180} nanorods in SI–DBP reached approximately 9.57×10^{-7} Au rods/μm^3 SI–DBP (Fig. 4). This concentration was very close to the observed density of domains in this sample (5.39×10^{-7} μm^{-3}). We infer that dilute suspended nanorods are very effective nucleants for ellipsoidal domains. However, within experimental error, the density of seeded domains did not increase when the concentration of nanorods was increased beyond this switching value. The density of heterogeneous primary nucleation events typically increases with added nucleant [38,39], as long as the nucleant is well dispersed and the nucleation efficiency does not change. In the material described in this report, greater nanorod concentrations may lead to aggregation, fusion or damage to the rods that decrease their nucleation efficiency in SI–DBP. This is consistent with optical microscope images of samples containing high concentrations of nanorods, in which dark flecks of Au aggregates were observed in the sample (Fig. 2).

3.2. Characterization of SIS–PS–Au nanorod composites: SAXS, polarized microscopy, and TEM analyses

Although we attempted to image nanorod-seeded domains in SI–DBP–Au by TEM, we found it difficult to prepare

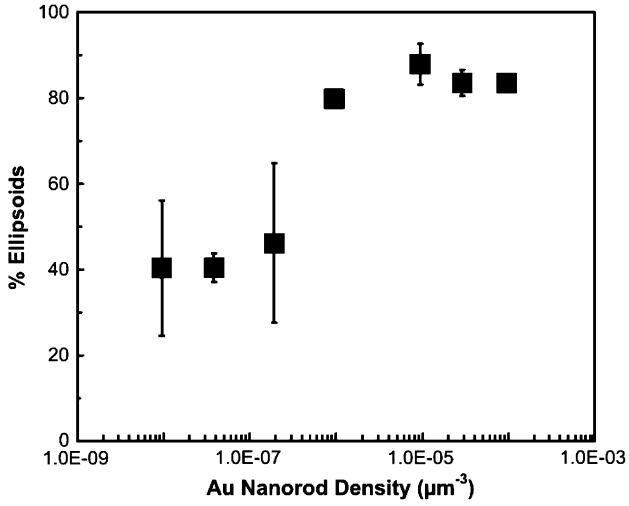

Fig. 4. Variation in percentage ellipsoid domains with concentration of $C_{12}H_{25}S$–Au_{180} nanorods in SI(18-12)–DBP.

microtomed sections of the material due to its fluidity. As an alternative, we investigated Au nanorod domain seeding in bulk SIS triblock copolymer. SIS is a thermoplastic elastomer used in a variety of commercial applications [40,41]. Cylinder-phase SIS monoliths can exhibit anisotropic elastic modulus when the mesophase is aligned throughout the bulk material by shear or thermal annealing [42,43]. We hoped to use nanorod orientation of SIS domains as a demonstration of the potential impact of domain templating on bulk, or at least localized, anisotropic mechanical properties. However, it is difficult to grow uniform mesophase domains in pure SIS; because of its high viscosity, the material must be cooled very slowly through T_{ODT}, and this temperature is high enough (>280 °C) that the polymer gradually decomposes throughout the cooling process. Vaidya et al. [44] and Mykhaylyk et al. [45] have shown that, when SIS is blended with a low molecular weight PS homopolymer, the blend forms highly ordered cylinder domains at lower T_{ODT} (215 °C for SIS with $f_{styrene} = 0.16$, diluted with 14 wt% PS with $M_n = 1000$ g/mol) via an intermediate, lattice-disordered phase. We combined $C_{12}H_{25}S-Au_{180}$ nanorods with this SIS–PS blend, using the same protocol developed for SI–DBP, and examined the effect of the nanorods on copolymer organization when cooled from the melt. SAXS measurements of SIS–PS prior to compositing with Au nanorods showed first- and second-order Bragg diffraction peaks at q^* and $\sqrt{3}q^*$, respectively, confirming a distinct cylindrical-phase morphology with a d-spacing of 29.8 nm (Fig. 5). SAXS measurements of SIS–PS–Au_{180} composite samples showed strong scattering from Au nanorods that masked the higher-order diffraction peaks, making it difficult to verify the sample's morphology. However, the principle Bragg diffraction peak (q^*) was clearly visible and showed the same domain d-spacing as the pure SIS–PS blend.

We were unable to observe domain growth in SIS–PS by polarized optical microscopy in the same way as we did for SI–DBP, because the domains in SIS–PS were much smaller. POM images of the SIS–PS blend both before and after compositing with Au_{180} nanorods (Fig. 6) showed small regions of birefringence, but it was difficult to distinguish domain boundaries in the images. As a result, although it was possible to locate the individual nanorods in these samples as we did for SI–DBP–Au_{180} [24], we could not relate the positions or orientations of these rods to specific nucleation of any single domain in the material. In general, block-copolymer domain size can be limited by the rate of grain growth, which is negatively affected by polymer's molecular weight and mobility [9,46–48], and these factors probably constrained the size of coherent domains observable by POM in SIS–PS.

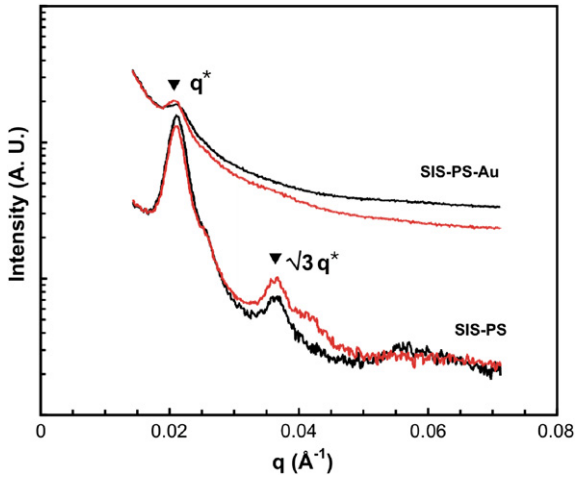

Fig. 5. SAXS profiles for a pure SIS–PS blend and an SIS–PS–Au_{180} composite samples. Samples were measured at room temperature (black curves) and 120 °C (red curves). The principle Bragg diffraction peak (q^*) was more discernible for SIS–PS–Au_{180} samples that were annealed and measured at 120 °C ($T > T_{g,PS}$).

TEM images of microtomed SIS–PS–Au_{180}, on the other hand, clearly showed the relationship between nanorod orientation and local mesophase order. TEM micrographs of SIS–PS and SIS–PS–Au_{180} that had been slowly cooled from isotropic to $T < T_{ODT}$, microtomed onto TEM grids, and exposed to OsO_4 showed a distinct pattern of alternating light PS domains and dark OsO_4-stained PI domains (Fig. 7a,b) that is consistent with a hexagonal (cylinder) morphology. Although previous studies show that thiol–Au bonds are labile at elevated temperatures [49,50], we did not observe any changes in the final morphology of SIS–PS–Au_{180} composite materials that might be attributed to alkanethiols thermally desorbed from the nanorods. In the nanorod-filled samples, polymer-embedded nanorods were easily distinguished as extremely dark objects in the TEM images. Nearly all nanorods were observed in the microtomed cross-section as elongated slices where the microtome knife has cut through the nanorod at an angle. We have assumed that the orientation of the larger nanorod in the sample was the same as the long axis of the sliced nanorod fragment. In general, these images showed that the PS cylinders in the domain surrounding each Au nanorod were primarily aligned parallel to the rod (Fig. 7c,d). Approximately 50% of polymer-embedded Au nanorods sampled were found to be surrounded by successive layers of cylinder domains that were within 10° of the Au nanorod (Figs. 7e and S1, [27]), and 30% were within 5°. These probabilities are much greater than would be expected from a random distribution of domain and nanorod orientations (11% within 10°, 5.5% within 5°). For Au nanorods surrounded by coaxially oriented, cylinder-phase domains, the coherent domain alignment was observed to propagate over large distances (>500 nm) into the surrounding polymer matrix without losing correlation with the templating Au nanorod surface. The co-alignment of cylindrical nanostructures with embedded nanorods was also preserved when different regions of the surrounding polymer matrix were scanned under the electron microscope (Fig. S13) [27].

Experimental observations of SI–DBP and SIS–PS Au nanorod composites support the hypothesis that nanorods can selectively nucleate uniform mesophase domains in cylinder-phase block copolymers. The extent to which homogeneously aligned cylindrical domains propagate from the seeding nanorod surface is determined by the typical domain size in the material—as large as 200 μm for low-viscosity

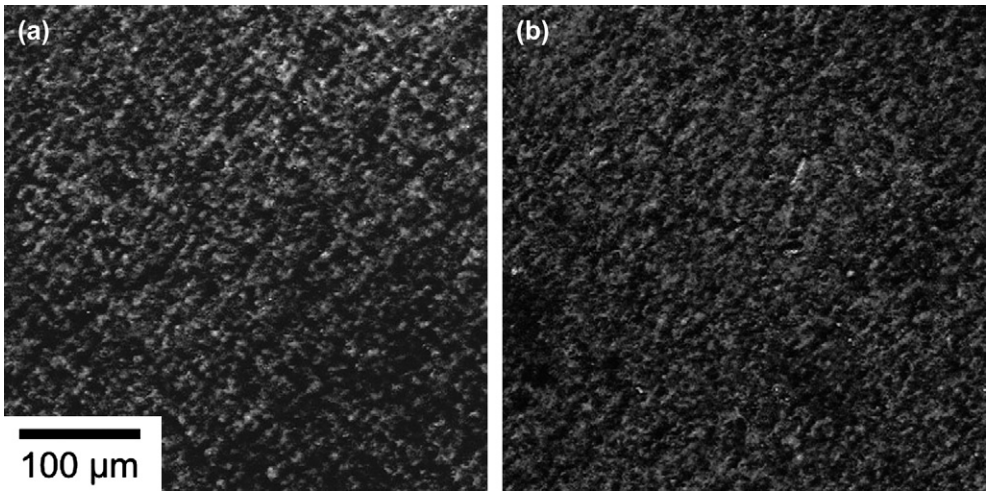

Fig. 6. Polarized optical microscopic images of SIS–PS (a) before and (b) after adding $C_{12}H_2S$–Au_{180} nanorods. Domains were nucleated by cooling samples from 215 °C ($T \sim T_{ODT}$) to 25 °C at 0.10 °C/min.

SI–DBP, but smaller for high-viscosity SIS–PS. However, these experiments do not provide mechanistic details on *how* these domains are nucleated at the nanoscale. We previously assigned specific roles to the dodecanethiol-modified nanorod surface, the PI block of the copolymer, and surface curvature to explain domain seeding in SI–DBP–Au [24]. The experiments described above indicate that some of these effects may be less critical than we first envisioned. To explore the range of conditions that might lead to coaxial domain nucleation at nanorod surfaces, and to better understand the nanostructural details of the nucleation process, we turned from experimental studies to theoretical mesoscale modeling.

3.3. Mesoscale modeling

There have been very few experimental studies on the kinetic mechanism of selective mesophase nucleation in block copolymers. Register and coworkers examined the kinetic effect of substrate step edges on the organization of ''two-dimensional'' microdomains in block-copolymer thin films [51–53]. Krishnamoorti et al. have also made conclusions about kinetic seeding of block-copolymer microstructure by dispersed clay particles based on final composite structures [20,21]. By contrast, there has been a great deal of recent experimental work on using thermodynamic constraints to control the morphologies of block-copolymer nanocomposites, typically involving strong segregation and/or annealing over long periods of time [54]. Theoretical studies on block-copolymer nanocomposite morphologies have also focused almost entirely on thermodynamics [55–60]. In these past theoretical works, the thermodynamic interactions between the nanostructure and the different polymer blocks, as well as complementarity between the scale and symmetry of the dispersed nanostructures and the block-copolymer repeat units, play important roles in determining the thermodynamically favored composite structure. Considering these past works, our observation that a 400 nm diameter rod could template the organization of 22 nm diameter cylinders of copolymer, regardless of surface treatment, was somewhat surprising.

To illustrate the kinetic effects of nanorod fillers on block-copolymer domain seeding, and to test the hypothesis illustrated in Scheme 1, we simulated the cooling of a block-copolymer melt in the presence of a rod-shaped object using dynamic density functional theory (DDFT) [61–66]. Sevink et al. have previously used this method to investigate the response of lamellar-phase diblock copolymers to embedded nanoshapes [66]. Using this same model, we investigated the effects of nanorod diameter and polymer–surface interactions on a model cylinder-phase copolymer in order to propose a general mechanism for domain seeding by one-dimensional objects. As outlined in our previously published report [24], an SI matrix was simulated as Gaussian bead strings with composition A_3B_7 (A = PI, B = PS) confined within a rectangular box. The box also contained a nanorod particle at the center. The initial state of each simulation was set such that the distribution of polymer segments was random, but as the simulation progressed the copolymer gradually segregated in response to the nanorod, the temperature, and the characteristics of the polymer blocks.

In the first set of simulations, energetic interactions between A beads and the nanorod surface were chosen to model preferential attraction of PI segments to alkanethiol-modified Au nanorods. The initial time evolution of domain phase segregation ($t = 200$ steps) showed the attraction of A beads to the surface initiated formation of a thin A bead wetting layer around the nanorod (Fig. 8). The wetting layer simultaneously templated the successive lamellae around the nanorod particles during the early stages of phase segregation ($t = 200$ steps). Rather than exhibiting a clear transition temperature, both the copolymer adsorption at the nanorod surface and successive lamellar templating occurred well above the T_{ODT} for the bulk material, and increased in extent as the simulation

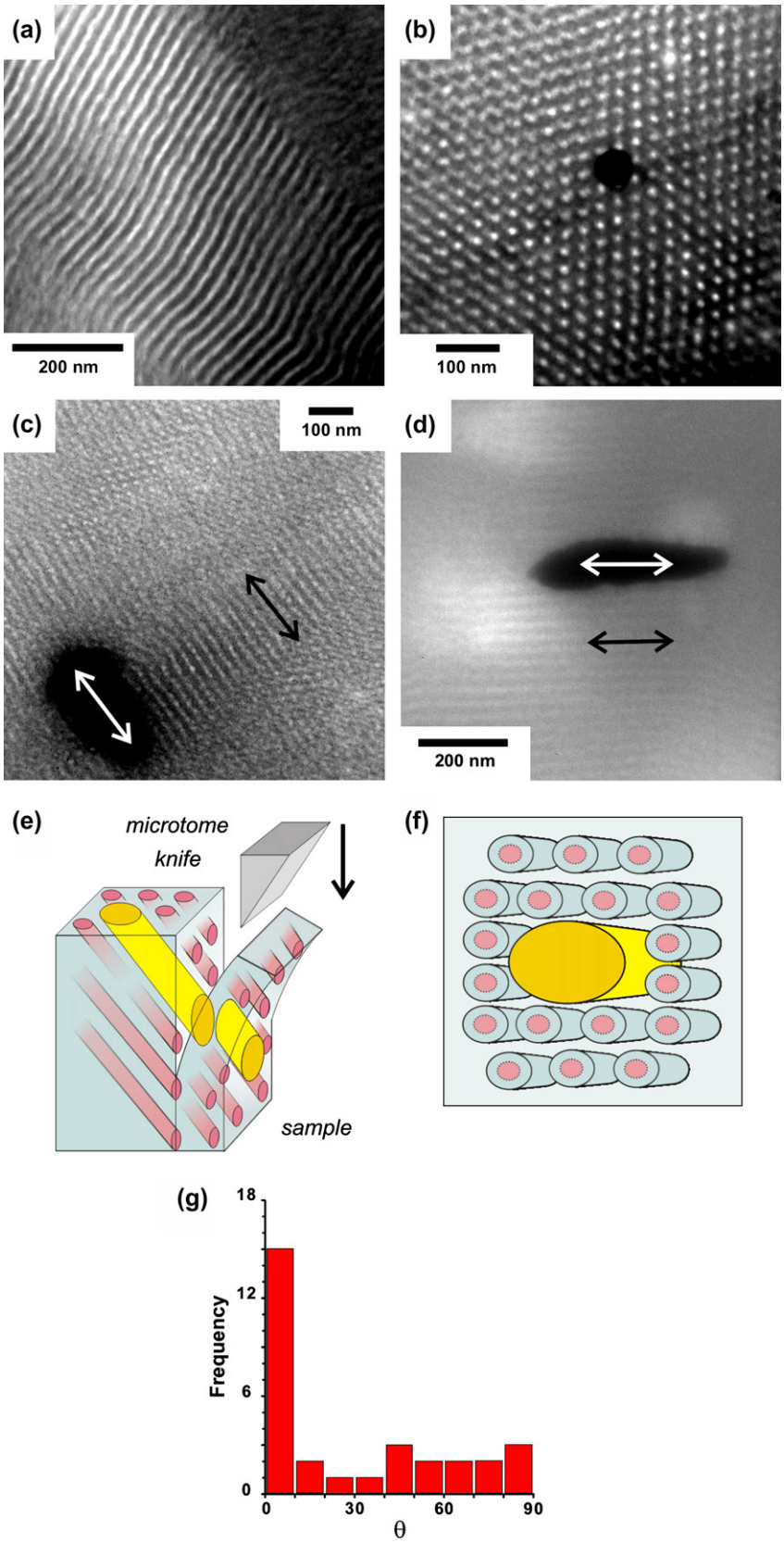

Fig. 7. (a,b) TEM images of cylindrical domains in microtomed SIS–PS, where hexagonally packed PS cylinders are oriented (a) parallel and (b) perpendicular to the plane of the micrograph. The PS domains appear light and PI domains appear dark due to staining of PI segments with OsO_4. (c,d) TEM images of SIS–PS–Au_{180}. The white and black arrows point out the relative orientation of Au nanorod nucleants and block-copolymer cylinders, respectively. (e,f) Illustration of features observed in a TEM image of a microtomed copolymer slice. (g) Histogram showing the distribution of angle differences between the orientation of Au nanorods and block-copolymer cylinders. A total of 31 Au nanorods were sampled to obtain the data shown in the histogram (Fig. S1) [28].

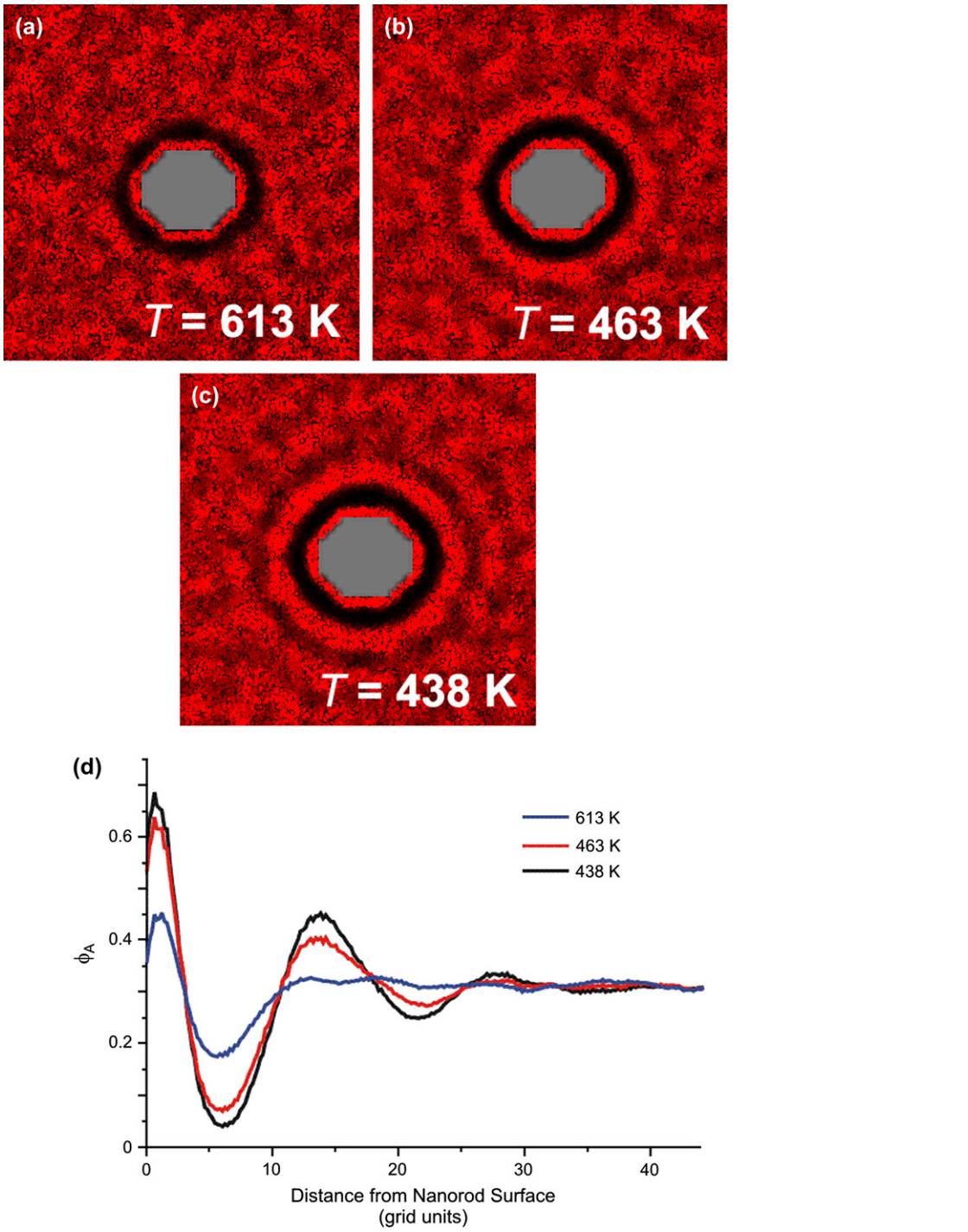

Fig. 8. (a–c) Distribution of A beads for a cylindrical-phase A_3B_7 copolymer melt in the presence of a nanorod particle at (a) $T = 438$ K, (b) 463 K, and (c) 613 K, when the DDFT simulation was allowed to proceed to dimensionless time step, $t = 200$. Beads are colored red, and the seeding nanorod is colored gray. (d) Graphical representation of the data shown in (a–c).

temperature was decreased (Fig. 8b,c). This trend was consistent with both experimental work [67–69] and mean-field theory [70] on progressive block-copolymer assembly at flat surfaces.

When the A_3B_7 copolymer was allowed to order below T_{ODT}, lamellar ordering at the nanorod surface was followed by conversion of the lamellae to cylinders and segregation of the bulk copolymer into ordered cylindrical mesophase. This sequence of events occurred in the simulations for a wide range of nanorod diameters (Fig. 9), confirming our experimental observation that cylinder-phase domains in SI–DBP could be seeded by different Au nanorod sizes. There were some variations in the simulations with nanorod diameter. For example, as the ratio of templating nanorod diameter

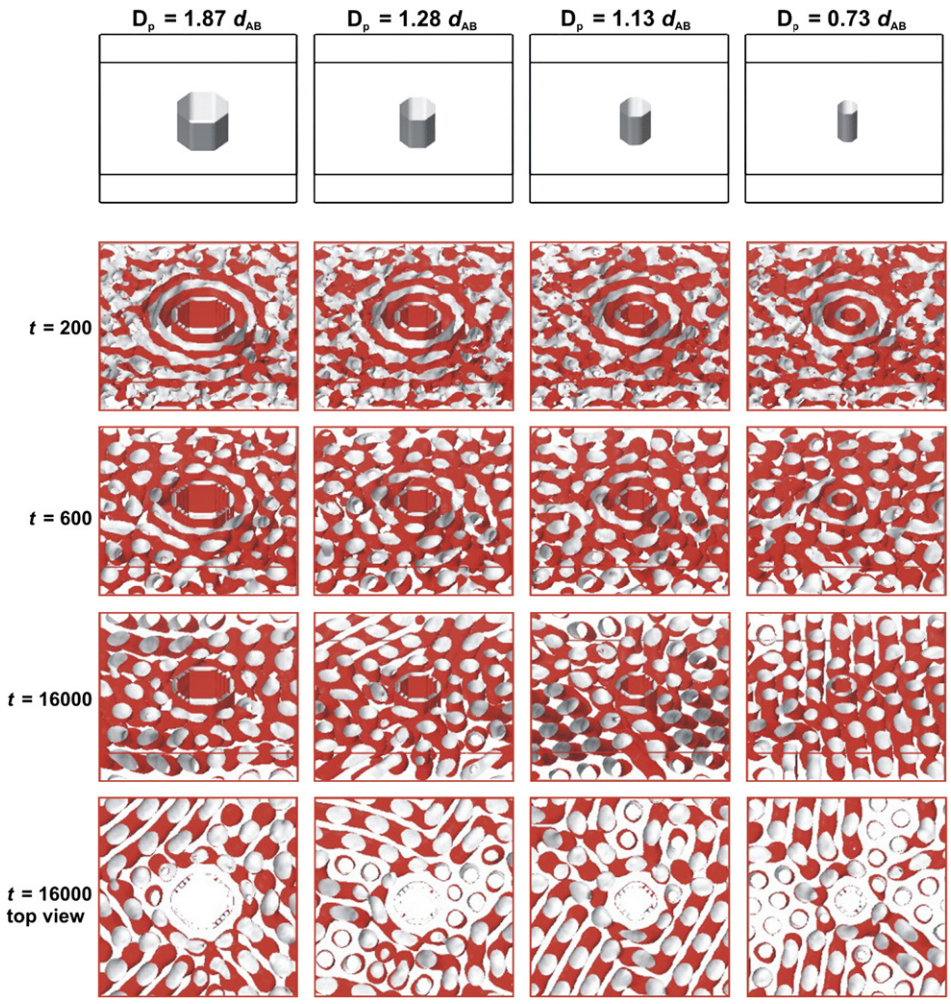

Fig. 9. Isodensity surfaces of A beads for a cylindrical-phase A_3B_7 copolymer melt with domain spacing d_{AB}, in the presence of nanorods with diameters D_p, at various dimensionless time steps t. Simulations of copolymer melt assembly on surfaces of nanorods with larger diameters were also performed for comparison [28].

D_p to copolymer phase periodicity d_{AB} was decreased from 1.87 to 0.73, the number of surface-templated lamellae also decreased. In addition, although the simulations sometimes yielded perfectly coherent alignment of copolymer cylinders with the templating rod [24], the templated cylinders were more often imperfectly registered with the nanorod orientation. It is not clear why this occurred, but we did observe in cases of misregistry that the bulk copolymer segregated near the same time as the polymer near the nanorod. This occurred more frequently in the simulation when the diameter of the nanorod was much larger than the copolymer phase periodicity (Figs. S2–S4, [27]). Our experiments showed that nanorod templating persisted at large values of D_p, which is somewhat inconsistent with these modeling results; we propose that the DDFT simulations did not always accurately represent the dynamics of block-copolymer phase segregation during long-range ordering.

To better understand how nanorods with different chemical surface treatments influence the evolution of order in our model block-copolymer system, we simulated the ordering of an A_3B_7 block copolymer in the presence of a nanorod with varying surface–polymer interactions. In our simulations, the surface–polymer interaction parameter ε_M was varied from -8 to 10 (Fig. 10) to adjust the attraction of each constituent block with the nanorod surface. For $\varepsilon_M < 0$, the nanorod was selectively wet by block A, and for $\varepsilon_M > 2$ by block B (Fig. 10, $t = 200$ steps). When the A and B beads were both set to have no enthalpic preference for the nanorod surface ($\varepsilon_{AM} = \varepsilon_{BM} = 0$), the nanorod was coated with an A bead wetting layer, presumably due to an entropic preference for the shorter A block to wet the nanorod surface [64]. In all of these cases, further lamellae were templated by this initial wetting layer. When the surface–polymer interaction was set to $\varepsilon_M = 2$, a transition point was reached where formation of the wetting layer and lamellae around the nanorod did not occur. Because ordering of the A_3B_7 block copolymer was successfully templated around the nanorod for different surface–polymer interactions, these results support our experimental observations of domain seeding by Au nanorods with different chemical surface treatments.

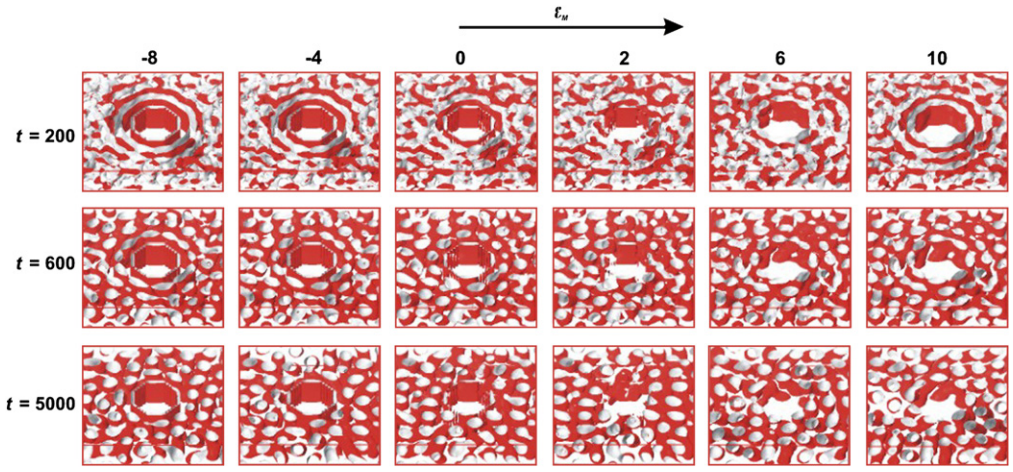

Fig. 10. Isodensity surfaces of A beads for a cylinder-phase A_3B_7 copolymer melt in the presence of nanorods with different polymer–surface interaction parameters, ε_M ($\varepsilon_M = \varepsilon_{AM} - \varepsilon_{BM}$). For $\varepsilon_M = 0$, A and B bead surface interactions were set to zero ($\varepsilon_{AM} = \varepsilon_{BM} = 0$).

4. Conclusions

Overall, the experimental and mesoscale modeling results described here illustrate a general mechanism for the kinetic templating of block-copolymer domains from nanoparticle seeds. There is broad interest in developing design rules for block-copolymer nanocomposites, and we stress that both thermodynamic and kinetic factors need to be considered in these rules. This is especially true when the size or slow mobility of dispersed nanoparticles prevents them from segregating to component copolymer blocks, as is the case for the large nanorods studied here. We also suggest that, if electric, magnetic, or shear fields were applied to align nanorods suspended in an isotropic polymer melt prior to domain nucleation, then this method might be used to actively orient block copolymers via kinetic templating throughout the bulk composite (as has been demonstrated for mesophases of nanorods and polymeric liquid crystals) [71–74].

Acknowledgements

We thank the Research Corporation (Research Innovation Award RI0964) and the Alfred P. Sloan Foundation (Fellowship BR-4527 to T.A.T.) for financial support of this research. The computational modeling was supported in part by the University of Minnesota Supercomputing Institute.

Appendix A. Supplementary data

Supplementary data associated with this article can be found in the online version, at doi:10.1016/j.polymer.2006.12.056.

References

[1] Hamley IW. The physics of block copolymers. Oxford: Oxford University Press; 1998.
[2] Bates FS, Fredrickson GH. Annu Rev Phys Chem 1990;41:525–57.
[3] Lodge TP. Macromol Chem Phys 2003;204:265–73.
[4] Chastek TQ, Lodge TP. Macromolecules 2004;37:4891–9.
[5] Balsara NP, Garetz BA, Chang MY, Dai HJ, Newstein MC, Goveas JL, et al. Macromolecules 1998;31:5309–15.
[6] Hashimoto T, Sakamoto N. Macromolecules 1995;28:4779–81.
[7] Hashimoto T, Sakamoto N, Koga T. Phys Rev E 1996;54:5832–5.
[8] Kim WG, Chang MY, Garetz BA, Newstein MC, Balsara NP, Lee JH, et al. J Chem Phys 2001;114:10196–211.
[9] Kim WG, Garetz BA, Newstein MC, Balsara NP. J Polym Sci Part B Polym Phys 2001;39:2231–42.
[10] Sakamoto N, Hashimoto T. Macromolecules 1998;31:3292–302.
[11] Kim SO, Solak HH, Stoykovich MP, Ferrier NJ, de Pablo JJ, Nealey PF. Nature 2003;424:411–4.
[12] Yang XM, Peters RD, Nealey PF, Solak HH, Cerrina F. Macromolecules 2000;33:9575–82.
[13] Wilmes GM, Durkee DA, Balsara NP, Liddle JA. Macromolecules 2006; 39:2435–7.
[14] Cheng JY, Mayes AM, Ross CA. Nat Mater 2004;3:823–8.
[15] Rockford L, Mochrie SGJ, Russell TP. Macromolecules 2001;34: 1487–92.
[16] Rockford L, Liu Y, Mansky P, Russell TP, Yoon M, Mochrie SGJ. Phys Rev Lett 1999;82:2602–5.
[17] Segalman RA, Yokoyama H, Kramer EJ. Adv Mater 2001;13:1152–5.
[18] Ha Y-H, Thomas EL. Macromolecules 2002;35:4419–28.
[19] Ha Y-H, Kwon Y, Breiner T, Chan EP, Tzianetopoulou T, Cohen RE, et al. Macromolecules 2005;38:5170–9.
[20] Silva AS, Mitchell CA, Fu Tse M, Wang H-C, Krishnamoorti R. J Chem Phys 2001;115:7166–74.
[21] Krishnamoorti R, Silva AS, Mitchell CA. J Chem Phys 2001;115: 7175–81.
[22] Hasegawa N, Usuki A. Polym Bull 2003;51:77–83.
[23] Lee JY, Park MS, Yang HC, Cho K, Kim JK. Polymer 2003;44: 1705–10.
[24] Laicer CST, Chastek TQ, Lodge TP, Taton TA. Macromolecules 2005;38: 9749–56.
[25] Schoenenberger C, van der Zande BMI, Fokkink LGJ, Henny M, Schmid C, Krueger M, et al. J Phys Chem B 1997;101:5497–505.
[26] For 400-nm Au nanorods, the predominance of scattering over surface plasmon resonance absorption made it difficult to assign sample extinction exclusively to the nanorods (as opposed to other scattering impurities). As a result, extinction coefficients were not determined for these nanorods.
[27] See Supplementary Data for details.
[28] Arridge RGC, Folkes MJ. J Phys D Appl Phys 1972;5:344–58.
[29] Hahm J, Sibener SJ. Langmuir 2000;16:4766–9.
[30] Harrison C, Park M, Chaikin P, Register RA, Adamson DH, Yao N. Macromolecules 1998;31:2185–9.

[31] Karim A, Singh N, Sikka M, Bates FS, Dozier WD, Felcher GP. J Chem Phys 1994;100:1620–9.
[32] Liu Y, Zhao W, Zheng X, King A, Singh A, Rafailovich MH, et al. Macromolecules 1994;27:4000–10.
[33] van Dijk MA, van den Berg R. Macromolecules 1995;28:6773–8.
[34] Huang E, Rockford L, Tussell TP, Hawker CJ. Nature 1998;395:757–8.
[35] Huang E, Russell TP, Harrison C, Chaikin PM, Register RA, Hawker CJ, et al. Macromolecules 1998;31:7641–50.
[36] Mansky P, Russell TP, Hawker CJ, Pitsikalis M, Mays J. Macromolecules 1997;30:6810–3.
[37] Thurn-Albrecht T, Steiner R, DeRouchey J, Stafford CM, Huang E, Bal M, et al. Adv Mater 2000;12:787–90.
[38] Binsbergen FL. J Polym Sci Polym Symp 1977;59:11–29.
[39] Binsbergen FL, De Lange BGM. Polymer 1970;11:309–26.
[40] Holden G. Thermoplastic elastomers. 2nd ed. Cincinnati: Hanser Gardner; 1996.
[41] Holden G. Understanding thermoplastic elastomers. Cincinnati: Hanser Gardner; 2000.
[42] Honeker CC, Thomas EL. Chem Mater 1996;8:1702–14.
[43] Folkes MJ, Keller A. Polymer 1971;12:222–36.
[44] Vaidya NY, Han CD, Kim D, Sakamoto N, Hashimoto T. Macromolecules 2001;34:222–34.
[45] Mykhaylyk TA, Mykhaylyk OO, Collins S, Hamley IW. Macromolecules 2004;37:3369–77.
[46] Chastek TQ, Lodge TP. J Polym Sci Part B Polym Phys 2006;44:481–91.
[47] Yamaguchi D, Hashimoto T, Vaidya NY, Han CD. Macromolecules 1999;32:7696–9.
[48] Bodycomb J, Funaki Y, Kimishima K, Hashimoto T. Macromolecules 1999;32:2075–7.
[49] Jain PK, Qian W, El-Sayed MA. J Am Chem Soc 2006;128:2426–33.
[50] Li Z, Jin R, Mirkin CA, Letsinger RL. Nucleic Acids Res 2002;30:1558–62.
[51] Trawick ML, Angelescu DE, Chaikin PM, Valenti MJ, Register RA. Rev Sci Instrum 2003;74:1390–2.
[52] Harrison C, Chaikin PM, Huse DA, Register RA, Adamson DH, Daniel A, et al. Macromolecules 2000;33:857–65.
[53] Harrison C, Adamson DH, Cheng Z, Sebastian JM, Sethuraman S, Huse DA, et al. Science 2000;290:1558–61.
[54] Bockstaller MR, Mickiewicz RA, Thomas EL. Adv Mater 2005;17:1331–49.
[55] Huh J, Ginzburg VV, Balazs AC. Macromolecules 2000;33:8085–96.
[56] Thompson RB, Ginzburg VV, Matsen MW, Balazs AC. Science 2001;292:2469–72.
[57] Thompson RB, Ginzburg VV, Matsen MW, Balazs AC. Macromolecules 2002;35:1060–71.
[58] Lee JY, Thompson RB, Jasnow D, Balazs AC. Macromolecules 2002;35:4855–8.
[59] Sides SW, Kim BJ, Kramer EJ, Fredrickson GH. Phys Rev Lett 2006;96:250601.
[60] Wang Q, Nealey PF, De Pablo JJ. J Chem Phys 2003;118:11278–85.
[61] Fraaije JGEM. J Chem Phys 1993;99:9202–12.
[62] Fraaije JGEM, Van Vlimmeren BAC, Maurits NM, Postma M, Evers OA, Hoffmann C, et al. J Chem Phys 1997;106:4260–9.
[63] Horvat A, Lyakhova KS, Sevink GJA, Zvelindovsky AV, Magerle R. J Chem Phys 2004;120:1117–26.
[64] Huinink HP, Brokken-Zijp JCM, van Dijk MA, Sevink GJA. J Chem Phys 2000;112:2452–62.
[65] Huinink HP, van Dijk MA, Brokken-Zijp JCM, Sevink GJA. Macromolecules 2001;34:5325–30.
[66] Sevink GJA, Zvelindovsky AV, van Vlimmeren BAC, Maurits NM, Fraaije JGEM. J Chem Phys 1999;110:2250–6.
[67] Menelle A, Russell TP, Anastasiadis SH, Satija SK, Majkrzak CF. Phys Rev Lett 1992;68:67–70.
[68] Green PF, Christensen TM, Russell TP. Macromolecules 1991;24:252–5.
[69] Anastasiadis SH, Russell TP, Satija SK, Majkrzak CF. Phys Rev Lett 1989;62:1852–5.
[70] Fredrickson GH. Macromolecules 1987;20:2535–42.
[71] Mrozek RA, Taton TA. Chem Mater 2005;17:3384–8.
[72] Mrozek RA, Kim B-S, Holmberg VC, Taton TA. Nano Lett 2003;3:1665–9.
[73] Dierking I, Scalia G, Morales P. J Appl Phys 2005;97:044309.
[74] Lynch MD, Patrick DL. Nano Lett 2002;2:1197–201.